Progress in Oceanography 112–113 (2013) 1–14

Contents lists available at SciVerse ScienceDirect

Progress in Oceanography

journal homepage: www.elsevier.com/locate/pocean

Controls of plankton production by pelagic fish predation and resource availability in the Alboran and Balearic Seas

Temel Oguz [a,b,*], Diego Macias [c,1], Lionel Renault [a], Javier Ruiz [c], Joaquin Tintore [a,d]

[a] SOCIB, Balearic Islands Coastal Ocean Observing and Forecasting System, Parc Bit, Naorte, Bloc A, Palma de Mallorca, Spain
[b] Middle East Technical University, Institute of Marine Sciences, 33731 Erdemli, Mersin, Turkey
[c] Department of Coastal Ecology and Management, Instituto de Ciencias Marinas de Andalucia (ICMAN-CSIC), Avd. Republica Saharauis/n, CP11510 Puerto Real, Cadiz, Spain
[d] IMEDEA (CSIC-UIB), Miquel Marquès 21, 07190 Esporles, Spain

ARTICLE INFO

Article history:
Received 2 March 2012
Received in revised form 7 March 2013
Accepted 7 March 2013
Available online 17 March 2013

ABSTRACT

A one-dimensional coupled physical and intermediate-complexity biochemical model comprising large and small phytoplankton and zooplankton groups, particulate organic nitrogen, ammonium and nitrate was developed to study the physical–biogeochemical interactions and parameters that control plankton production in the Alboran and Balearic Sea ecosystems. The model findings suggest that pelagic fish predation and resource availability through lateral and vertical nutrient inputs jointly characterize the plankton community structures. In agreement with previous observations, a typical annual plankton structure of the mesotrophic systems involves a vertically homogeneous biomass of large groups of phytoplankton and zooplankton within the upper 50-to-100 m layer from mid-November to April and a subsurface biomass accumulation distributed roughly within 25–75 m depths in the following months. Their light and temperature limitations constrain the smaller groups into the thermocline zone (25–50 m) during late spring and summer. These obtained results were dependent on the zooplankton actively switching between preys (i.e., the food preference coefficients dependent on prey biomass). In the case of no switching, spurious dynamic equilibrium solutions may arise in the case of a constant and weak fish predation rate and using the quadratic predation formulation. The choice of a Holling Type II (i.e., hyperbolic) predation function may, however avoid ambiguous representation of the annual plankton structure in the case of a constant food preference choice under relatively weak predation pressures.

1. Introduction

The Mediterranean Sea, generally recognized as an oligotrophic basin, possesses important geographical variations in terms of food availability (Bosc et al., 2004; Barale et al., 2008; D'Ortenzio and d'Alcala, 2009; Siokou-Frangou et al., 2010; Navarro et al., 2011). In general, productivity in the western basin exceeds that in the eastern basin. On a regional scale, the Alboran, the Balearic, the northern Adriatic, and the Northern Aegean Seas always appear to be biologically more productive sub-basins than other regions, and on local scales there are even more pronounced hotspots of biological production connected to river runoff, submarine canyons, and regional upwelling centers (e.g., Gulf of Lions, the northwestern Alboran Sea, the Ebro delta and the Catalan shelf-slope zone, and the Nile and Po deltas).

The northwestern (NW) Alboran Sea along the Spanish coast between 5.0°W and 3.5°W longitudes (Fig. 1) supports high biological productivity due to enhanced lateral and vertical nutrient fluxes (Ramírez et al., 2005; Reul et al., 2005; Mercado et al., 2007; Macías et al., 2008). The region also sustains one of the richest fish resources in the Mediterranean (Bellido et al., 2008) and serves as a favourable habitat and nursery ground for the European sardine (*Sardina pilchardus*) and European anchovy (*Encraulis encrasicolus*) (Estrada, 1996; García-Lafuente et al., 1998; Rubín et al., 1999; García et al., 2003; Macías et al., 2011). These small pelagics fishes also serve as a rich food source for apex predators (Coll et al., 2011). Enhanced biological activity declines toward the interior of the oligotrophic Western anticyclonic Alboran Gyre (WAG) and as the Atlantic jet proceeds eastward (e.g. Tintore et al., 1991; Viudez et al., 1998). In general, the Almeria–Oran front (Tintore et al., 1988) lying along the eastern flank of the Eastern anticyclonic Alboran Gyre (EAG) separates the relatively productive Alboran Sea from the less productive western Algerian basin. The oligotrophy of the latter system is related to the very limited vertical and lateral supply of nutrients into the photic layer throughout the year.

* Corresponding author at: SOCIB, Balearic Islands Coastal Ocean Observing and Forecasting System, Parc Bit, Naorte, Bloc A, Palma de Mallorca, Spain.
E-mail address: oguz@ims.metu.edu.tr (T. Oguz).
[1] Present address: European Commission, Joint Research Center, Institute for Environment and Sustainability, Water Research Unit, Via E. Fermi 2749, 21027-Ispra, Italy.

0079-6611/$ - see front matter © 2013 Elsevier Ltd. All rights reserved.
http://dx.doi.org/10.1016/j.pocean.2013.03.001

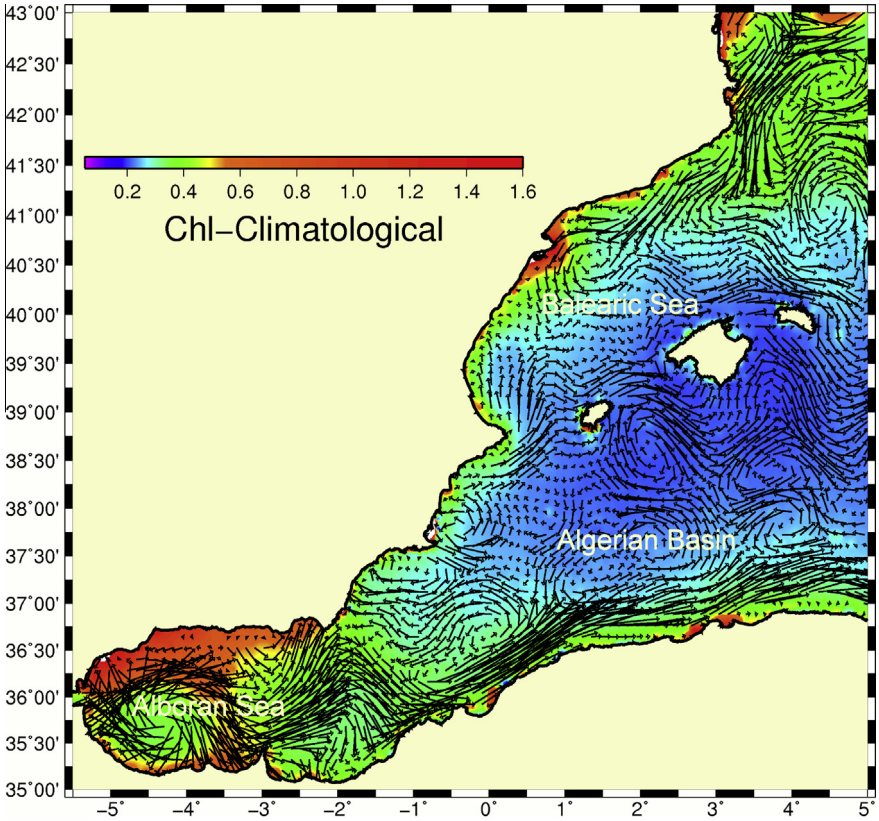

Fig. 1. Surface chlorophyll concentration (mg m^{-3}) distribution provided by averaging of 9 km monthly SeaWiFS products for 1998–2010 and the geostrophic currents estimated from the altimeter SSH data for 1993–2010. The chlorophyll concentration data are retrieved from http://reason.gsfc.nasa.gov/OPS/Giovanni/ocean.seawifs.2.shtml and the altimeter SSH data are obtained by the daily gridded AVISO products available at http://ftp.aviso.oceanobs.com//donnees/ftpsedr/DUACS/regionalmfstep/dt/upd/madt/merged/h/.

This regional variability along with the major circulation features are depicted in Fig. 1.

The monthly climatological surface chlorophyll-a (Chl-a) concentrations inferred from ocean color data for the Alboran Sea (García-Gorriz and Carr, 1999; Macias et al., 2007) suggest relatively low chlorophyll values of approximately 0.5 mg m^{-3} during the summer months (June–September) followed by a gentle increase up to 0.8 mg m^{-3} during autumn (from September to December) that intensifies to an average concentration greater than 0.9 mg m^{-3} by the end of winter and the beginning of spring (February–April) and then decrease afterwards to the lower summer values. The measurements performed along the Spanish coast of the NW Alboran Sea in 2002 (Ramírez et al., 2005) further point to the role of wind-driven upwelling events and associated relatively high Chl-a concentrations of approximately 2.0 mg m^{-3} during April (Fig. S1a), which are also associated with a relatively high nitrate (NO_3) concentration (~2.0 μM on average) near the surface (Fig. S1b). From this moment onwards, surface nitrate concentration is reduced to less than 0.5 μM, and the Chl-a peak decreased to 1.5 mg m^{-3} in summer and 1.0 mg m^{-3} in autumn with a progressive deepening of its position towards the nitracline between 45 and 75 m (Fig. S1a). During the winter, the chlorophyll maximum layer attains vertically uniform values in the 0.5–0.75 mg m^{-3} range near the surface. A complementary set of measurements along the offshore transect toward the interior of the western Anticyclonic Gyre (Reul et al., 2005) also revealed high values up to 3 mg m^{-3} within the upper 40 m layer in July and December 1996. Low chlorophyll values of approximately 0.2 mg m^{-3} at 75 m generally define the lower boundary of the subsurface productive layer. The nitrate measurements reveal a steep linear increase up to the 6–7 μM range at 100 m and a more gradual rise to the 7.0–7.5 μM range at 200 m and the 8–9 μM range at 300 m (Fig. S1b).

The quasi-permanent cyclonic gyral circulation between the Catalan and Balearic frontal zones of the Balearic Sea characterizes another relatively productive system (Fig. 1) (Latasa et al., 1992; Estrada et al., 1993; Estrada, 1996; Masó et al., 1998; Alcaraz et al., 2007). The cyclonic gyral circulation regime in the Balearic Sea differs from that in the Alboran Sea in terms of a weaker density stratification due to a limited intrusion of the Atlantic water mass (Alcaraz et al., 2007). Its biological production is locally driven by the vertical processes and laterally by the occasional intrusion of the nutrient-rich water mass of the Ligurian–Provencal basin by mesoscale features and the intermittent flow bifurcations of the Catalan current (Salat, 1996). Production therefore decreases gradually southward with an inflow of oligotrophic surface water from the Algerian basin. Nevertheless, the annual Chl-a concentration distribution in the northern parts of the Balearic basin has a similar annual structure and reveals a vertically homogeneous layer of 2–3 mg m^{-3} within the upper 75 m layer during the winter months (Fig. S1c). It is followed by the spring–summer subsurface layer with 1–2 mg m^{-3} Chl-a concentration (Fig. S1c).

The available modeling studies of the Alboran and Balearic Seas have been limited to the aggregated representation of all phytoplankton and zooplankton groups and thus the NPZD-type food web configuration. The one-dimensional biogeochemical model by Bahamón and Cruzado (2003) provided a general assessment of the effect of a different supply of nitrogen and irradiance on the phytoplankton primary production and the zooplankton secondary production along the Catalan coast of the Balearic Sea.

The model emphasized a strong control of the late winter and the early summer subsurface phytoplankton biomass by zooplankton grazing. This same model also linked the deep chlorophyll maximum (DCM) layer to nutricline depth variation. Macías et al. (2011) utilized a three-dimensional, four compartment (NPZD type) ecosystem model coupled with a hydrodynamic model. It was used to explain the impact of atmospheric forcing on the physical and biogeochemical environment of the inner shelf region of the northwestern Alboran Sea and the subsequent plankton production on spawning success of the small pelagic fish population in July 2008. Macías et al. (2010) emphasized the critical role played by the frequency of nutrient fluxes from the Gibraltar Strait on the total biomass and community composition of plankton in the upper, lit water layer of the NW Alboran Sea. A three-dimensional coupled model of the Alboran Sea (Skliris and Beckers, 2009) identified several hot spots of high biological productivity in the region without elaborating their specific governing mechanisms and processes. These modeling studies provide a limited contribution to our understanding of the roles of various physical and biological processes on the Alboran and Balearic Sea ecosystems. In particular, a systematic assessment of the relative roles of bottom-up and top-down controls in different ecological conditions demands more extensive modeling studies using a more sophisticated model food web configuration.

The present study constitutes part of our ongoing efforts to develop a community-based, intermediate complexity physical-biochemical modeling system in both 1-D and 3-D settings to address the impacts of the circulation dynamics, climate change, eutrophication and fishing on the biological productivity of the region. This study focuses on the one-dimensional version of the model and documents the sensitivity of the food web structure to the regional physical conditions. In particular, the main observed biological characteristics are simulated in three contrasting sites by altering only the upwelling velocity and vertical and horizontal nitrate fluxes, while all the other model parameters are assigned fixed values. These contrasting sites are the highly productive NW Alboran Sea to the east of the Gibraltar strait, the moderately productive conditions observed in the cyclonic gyral circulation of the Balearic Sea and in the central Alboran Sea, and the oligotrophic system of the Alboran anticyclonic gyres. The present study further documents how to parameterize zooplankton grazing for a realistic representation of the annual plankton structure and how to avoid the development of spurious lower trophic level food web structures that may likely arise for some range of fish predation rate values and the choice of constant food preferences.

The present study is organized as follows. The general framework of physical and biochemical model structures, their initial and boundary conditions, and the specification and calibration procedures of the biological model parameters are described in Section 2 with additional details provided in Appendix A. The first part of Section 3 covers the specific case studies for highly and moderately productive and oligotrophic conditions. The second part describes the response of the annual plankton structure to the zooplankton-grazing and fish-predation formulations. Discussion of the results and conclusions are presented in Section 4.

2. Materials and methods

2.1. Model formulation

The physical module is based on the one-dimensional version of the Princeton Ocean Model (POM), which solves temperature and salinity transport equations of the general form

$$\frac{\partial F}{\partial t} = \frac{\partial}{\partial z}\left(K_h \frac{\partial F}{\partial z}\right) \tag{1}$$

where F denotes either temperature or salinity, t is time, z is the vertical coordinate (positive upwards), ∂ denotes partial differentiation, and K_h is the vertical turbulent diffusion coefficient. For further details on the documentation of the model, we refer to its previous Black Sea implementation by Oguz et al. (1996). The vertical eddy diffusivity was computed by the Mellor–Yamada level 2.5 turbulence scheme. Numerical treatment of the equations followed the original three-dimensional POM code in the absence of horizontal advection, diffusion, and pressure gradient terms. Fifty-one vertical sigma levels were introduced to resolve the 200 m thick water column.

The local temporal variations of all state variables of the biochemical module are expressed by equations of the general form

$$\frac{\partial F}{\partial t} + HorAdv + (w - w_d)\frac{\partial F}{\partial z} = \frac{\partial}{\partial z}\left(K_h \frac{\partial F}{\partial z}\right) + R_F \tag{2}$$

where F denotes any state variable of the biological model, w is the vertical velocity, w_d signifies the downward sinking velocity, *HorAdv* parameterizes the horizontal advective fluxes in a 1-D context, R_F expresses biological sources and sinks for each of the state variables, and t, z, K_h and ∂ are as previously defined for the physical model. The vertical advection term involving w and the horizontal advection term *HorAdv* in the form of incoming and outgoing fluxes apply for the nitrate equation only. Additional specification of *HorAdv* to the phytoplankton and zooplankton equations was avoided so as not to introduce additional empiricism into the model. *HorAdv* and w are specified externally as input as described in the next section. The sinking term involving w_d applies to the large phytoplankton and detritus equations. The source-sink terms are described in Appendix A. The biochemical model is solved coupled with the physical model and using the same numerical methods.

Based on available observations (e.g., Rodríguez et al., 2001), the phytoplankton community is represented by large (microphytoplankton) and small (nanophytoplankton) groups with cell sizes larger and smaller than 20 μm that generally typify diatoms and flagellates, respectively. The availability of coccolithophores and dinoflagellates is considered as much less critical than the other major groups within within the annual phytoplankton community structure, although this assumption may not be strictly true for 1997–2002 in the NW Alboran Sea (Mercado et al., 2007). The zooplankton community is represented by microzooplankton (nominally <0.2 mm) and mesozooplankton (0.2–2 mm). The microzooplankton category includes heterotrophic flagellates, ciliates and juvenile copepods. The mesozooplankton category essentially consists of adult copepods. The link to higher predators is parameterized by the quadratic predation term (as the default setting) in the zooplankton equations. This term represents fish predation pressure as a continuous loss from the lower trophic food web structure (i.e., no recycling within the food web). Apart from its role in the closure of the model, it may further act as stabilizer of the model (Gibson et al., 2005). The model neglects the role of bacterioplankton and other components of the microbial food web because of the lack of data and also to keep the model as simple as possible for its 3-D implementation. The model thus preferentially sets the energy flow to the higher predators through (i) the small plankton size community structure (the nanophytoplankton and microzooplankton groups), and (ii) the large plankton size community structure (the microphytoplankton and mesozooplankton groups). These two primary food chains are interconnected with each other by additional energy flows among their members. Within the Alboran and Balearic Sea ecosystems, nitrogen is the most limiting nutrient for phytoplankton growth (Dafner et al., 2003; Ramírez et al., 2005; Mercado et al., 2007). The plankton dynamics are therefore complemented by the nitrogen cycle, which involves ammonium, nitrate, and particulate

organic nitrogen components. In the absence of bacterioplankton and dissolved organic nitrogen pool, detritus is remineralized directly to ammonium at a constant rate. This model structure is also called the N2P2Z2D model.

2.2. Initial and surface boundary conditions, lateral fluxes

2.2.1. Initial conditions

The model initially prescribes a stratified water mass structure representative of the autumn (October) conditions. The Alboran case is characterized by the fresher and warmer Atlantic water mass located above the colder and more saline water mass that is partly injected towards the surface by the permanent upwelling mechanism. Consistent with the autumn profiles provided by Ramírez et al. (2005), the Atlantic water mass is characterized by 19.0 °C temperature and 36.5 salinity at the surface and overlays Mediterranean water characterized as 13.0 °C, 38.0 at 100 m, and 12.5 °C, 38.5 at 200 m through a transitional (the so-called pycnocline) layer that is defined by 18.0 °C, 37.5 at 50 m. The Balearic case specifies a similar initial vertical temperature structure but with a slightly more saline water column within the upper 100 m layer. These initial water mass structures are accompanied by an idealized vertical nitrate structure of 1.5 μM within the first 50 m layer, 3.5 μM within the 50–100 m layer and 6.5 μM in the rest of the water column. This idealized nitrate structure transforms into its observed structure during the model spin-up phase. Thus, obtaining a vertical nitrate annual structure that is consistent with the observed one is a first to assess the model performance.

2.2.2. Surface forcing

The physical model for both the Alboran and Balearic Seas is forced by the same daily climatological surface temperature, salinity and an idealized wind stress, whereas no-flux conditions are specified at the bottom boundary. These data sets were compiled from various sources of published data. In the one-dimensional context, forcing of the model by temperature and salinity at the surface has an advantage in that it incorporates not only seasonal changes of the heat and fresh water fluxes but also the peculiarities of the regional water mass characteristics. For the Alboran Sea, the climatological surface salinity changes between 36.5 and 36.9 over the year with relatively higher values in winter and lower for summer. The climatological surface temperature presents a cyclic structure decreasing linearly from 23 °C at mid-July to 15.5 °C at the end of February and then increases linearly again during spring and summer. The climatological structure of the photosynthetically available radiation (PAR) changes from the maximum value 150 W m^{-2} at the beginning of August to its minimum value 25 W m^{-2} in November. It maintains this minimum value throughout the winter and starts increasing again by the end of February, at first steeply up to 100 W m^{-2} at the end of April and then more gradually to 150 W m^{-2} over the next 3 months (May–July).

2.2.3. Lateral and vertical nitrate fluxes

The default model simulations specify a year-round upwelling velocity in response to a series of wind-induced upwelling episodes (Bakun and Agostini, 2001; Mercado et al., 2007; Macías et al., 2008). It is set to 1 m d^{-1} for December–June (inclusive) to characterize the intermediate upwelling phase and reduced to 0.5 m d^{-1} during the summer–autumn to account for weaker upwelling (Bakun and Agostini, 2001). For the Alboran Sea simulations, a continuous lateral nutrient supply (NF_{in}) transported into the region by the Atlantic jet is prescribed within the upper 80 m water column. Following the observations of Macías et al. (2008), its default winter value for the January–June period was set to $NF_{in} = 0.8 \times 10^{-6}$ mmol N m^{-3} s^{-1}. It follows that $NF_{in} \sim u \cdot \Delta N/\Delta x$ with a typical current speed of the Atlantic jet $u \sim 0.5$ m s^{-1}, a typical distance to the Gibraltar entrance $\Delta x \sim 200$ km, and the corresponding difference of nitrate concentration $\Delta N \sim 0.3$ mmol m^{-3} (e.g., Macías et al., 2010). This value decreases by half during the rest of the year following the observed variability of the Atlantic inflow through the strait of Gibraltar (e.g., García-Lafuente et al., 1998).

As the upwelling mechanism continually pumps subsurface nitrate towards the surface, it has to partially leave the water column to avoid accumulation near the surface during the long-term integration period. This lateral outgoing flux (NF_{out}) is specified at a constant rate of 5×10^{-7} mmol N m^{-3} s^{-1} at all vertical levels above 150 m during the winter-spring period. It then is at half of its standard value for the rest of the year. Its magnitude and vertical extent were adjusted by trial-and-error to provide a vertical biochemical structure consistent with the observed nitrate and chlorophyll profiles.

2.3. Parameter setting and calibration

The upwelling velocity, the lateral incoming and outgoing nitrate fluxes, and the predation pressure rate constant form four specific free parameters for the model simulations considered in this study. Their combinations identify the relative strengths of top-down and bottom-up controls on the annual plankton structure. The rest of the model parameters are assigned to the fixed values compiled from the similar modeling studies as listed in Tables 1–3. They are adjusted for the present model through an extensive set of sensitivity studies that involved (i) finding the primary set of parameters that are most critical for model performance based on their initial guesses and literature values, (ii) changing these primary parameters set in different combinations within their ±25% range and finding the model-data misfits, and (iii) repeating this procedure until the parameter set provides results better than 85% of the observed monthly averaged nitrate and chlorophyll profiles within the euphotic layer for the reference simulation case. The simulations also ensure that these choices do not produce unstable oscillatory solutions. The default parameter set obtained by this procedure is listed in Tables 1–3. Further details of the way in which their values were chosen are described in Appendix A. The specific cases presented below are listed in Table 4.

3. Results

3.1. Case studies

3.1.1. The reference case: high biological productivity in the case of strong bottom-up and top-down controls

The simulation ALBA1 (Table 4) characterizes the conditions of relatively strong values for the Atlantic inflow, the upwelling velocity, and the fish predation pressure. It therefore represents the case of both strong bottom-up and top-down controls in the highly productive conditions of the NW Alboran Sea close to the Gibraltar strait.

The annual water column physical structure (Fig. 2a–c) illustrates pronounced seasonal changes. The temperature is coldest (14.0–15.0 °C) during January–March, after which the seasonal thermocline gradually builds up in the spring–summer within a 20–50 m layer below the warm surface mixed layer with a maximum temperature of 23 °C (Fig. 2a). The temperature changes from the 14.0–14.5 °C range at 75 m depth to 13.5 °C at 100 m and 13.0 °C at 125 m and 12.5 °C below the 150 m layer. Salinity varies from 36.9 in winter to 36.5 in summer (Fig. 2b). It reaches 38.0 at 100 m and 38.5 at 200 m. It generally follows the seasonal changes in the mixed layer depth as is clearly depicted by the vertical

Table 1
Definition of parameters and their values used for phytoplankton and zooplankton groups.

Definition	Large phyto	Small phyto	Microzoo	Mesozoo	References
Maximum growth/grazing rate (d^{-1})	$\sigma_l = 2.8$	$\sigma_s = 2.2$	$g_s = 1.0$	$g_l = 0.7$	a, c, d, j
Initial slope of the PI curve ($m^2\ W^{-1}$)	$\alpha_l = 0.32$	$\alpha_l = 0.30$			e, h
Mortality rate (d^{-1})	$m_{PL} = 0.04$	$m_{PLS} = 0.06$	$m_{ZS} = 0.06$	$m_{ZSL} = 0.05$	d, j
Excretion rate (d^{-1})			$\mu_s = 0.09$	$\mu_l = 0.05$	d, h, m
Assimilation efficiency			$\gamma_s = 0.80$	$\gamma_l = 0.70$	h, j, m
Half saturation constant (mmol N m^{-3})	$K_{nl} = 0.5$ $K_{al} = 0.5$	$K_{ns} = 0.3$ $K_{as} = 0.3$	$K_s = 0.7$	$K_l = 0.9$	d, h, j
Q_{10} parameter for temperature limitation	$Q_{pl} = 1.5$	$Q_{ps} = 2.0$	$Q_{zs} = 2.0$	$Q_{zl} = 1.5$	b, n

Table 2
Food capture efficiency parameters of zooplankton groups.[a]

	Microzoo	Mesozoo
Large phytoplankton	0.3	0.7
Small phytoplankton	0.6	0.2
Detritus	0.2	0.3
Microzooplankton	0.0	0.4

[a] They are tuned parameters based on the sensitivity studies to reproduce the observed seasonal biomass conditions.

structure of vertical diffusivity (Fig. 2c). The deepening of the mixed layer, not more than 70 m in winter (Fig. 2c), is due to the presence of strong salinity changes separating the Atlantic and Mediterranean waters between approximately 50 and 100 m depths. The simulated temperature and salinity vertical structures are in good agreement with these observations (Fig. S2a and b in Supplementary material). In terms of the lower trophic food web structure, it is important to emphasize the restriction of nutrient enrichment into the upper 75–100 m layer in response to shallow convective mixing under strong stratification (Fig. 2c).

The annual phytoplankton structure is formed by two different contributions (Fig. 3a and b). Starting in November and lasting until the end of April, the diatom-based large cell group, which is capable of growth at high nutrient and low light and temperature conditions, supports an increasing phytoplankton biomass within the gradually deepening mixed layer from 40 m to 75 m (Fig. 3a). In general, the vertical structure closely follows the changes in vertical diffusivity (Fig. 2c), indicating a new production-based phytoplankton biomass increase up to 0.9 mmol N m^{-3}, reaching its maximum intensity of 1.5 mmol N m^{-3} for a few weeks in March. This strong bloom phase coincides with the pronounced shallowing phase of the mixed layer due to the termination of strong vertical mixing within the water column (Fig. 2c) that counteracted the development of strong phytoplankton blooming earlier in winter. The surface-intensified bloom continues with decreasing intensity within the upper 50 m layer in April. This is expected to be related to the regenerated production provided by the recycling of nutrients following the intense March bloom. Because the model involves an explicit representation of the nutrient recycling process, it is not possible to precisely distinguish relative contributions of the new and recycled productions. Thereafter, the core of high biomass layer shifts roughly to the 25–50 m layer below the seasonal thermocline at the level of ~1.0 mmol N m^{-3} that extends with a declining intensity down to 100 m through the entire spring

Table 3
Definition of some parameters and their values.

Definition	Value	References
Light extinction coefficient for PAR in pure water (m^{-1})	$k_w = 0.05$	e, g
Self-shading coefficient due to phytoplankton and detritus (m^{-1} mmol N m^{-3})	$k_p = 0.02$	f, e, g
Nitrification rate (d^{-1})	$r = 0.08$	h, b,
Remineralization rate for particulate nitrogen (d^{-1})	$\varepsilon_n = 0.15$	h, k, a, j
Maximum phytoplankton sinking rate (m d^{-1})	$W_p = 2.0$	b, m
Maximum detritus sinking rate (m d^{-1})	$W_d = 8.0$	b, m
Half saturation constant of the light-regulated nitrification rate (W m^{-2})	$K_{PAR} = 10$	l
Half saturation constant of the detritus sinking rate (mmol N m^{-3})	$K_D = 0.5$	b
Predation rate of higher predators on zooplankton groups ((mmol N)$^{-1}$ m^3 d^{-1})	$f_P = 0.15$	f

(a) Ducklow and Fasham (1992), (b) Oguz et al. (1999), (d) Raybound et al. (2011), (e) Morán and Estrada (2001), (f) Travers and Shin (2010), (g) Mercado et al. (2007), (h) Kone et al. (2005), (i) Gibson et al. (2005), (j) Lima et al. (2002), (k) Rivierea and Pondaven (2006), (l) Gibson and Spitz (2011), (m) Denman (2003), (n) Bissinger et al. (2008).

Table 4
The list of model simulations with different combinations of the free parameters chosen in the model. Below, f_P denotes the predation rate of higher predators on the large and small zooplankton groups, W_{up} is the vertical velocity (positive upwards), NF_{in} is the nitrate input into the water column injected within the upper 80 m layer by the Atlantic jet, and NF_{out} represents the nitrate taken out per day from the water column within the upper 150 m layer in response to its upwelling and lateral input. Their default parameter values are set to $f_P = 0.15$ (mmol N)$^{-1}$ m^3 d^{-1}, $W_{up} = 1.0$ m s^{-1}, $NF_{out} = 5 \times 10^{-7}$ mmol N m^{-3} s^{-1}, $NF_{in} = 0.8 \times 10^{-6}$ mmol N m^{-3} s^{-1}.

Simulation	Fish predation	Upweling velocity	Outflux of nitrate	Influx of nitrate	Feeding coefficients
ALBA1	f_P	W_{up}	NF_{out}	NF_{in}	Variable
ALBB1	f_P	W_{up}	NF_{out}	$0.1 * NF_{in}$	Variable
ALBE2	$0.25 * f_P$	$-0.5 * W_{up}$	0	$0.1 * NF_{in}$	Variable
BAL1	f_P	W_{up}	NF_{out}	0	Variable
ALBA1c	f_P	W_{up}	NF_{out}	NF_{in}	Constant
ALBB3	$0.25 * f_P$	W_{up}	NF_{out}	$0.1 * NF_{in}$	Variable
ALBB3c	$0.25 * f_P$	W_{up}	NF_{out}	$0.1 * NF_{in}$	Constant

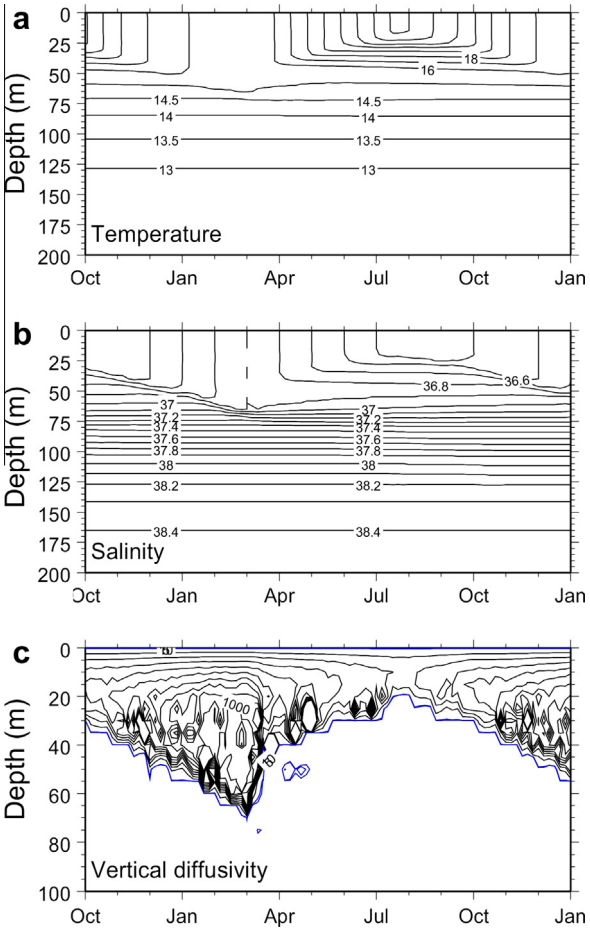

Fig. 2. Annual distributions of (a) temperature, (b) salinity, and (c) vertical diffusivity within the upper layer water column. Day 1800 corresponds to 1st October and the year lasts for 360 days at 2160. The additional 90 days between 2160 and 2250 represent the autumn period of the subsequent year.

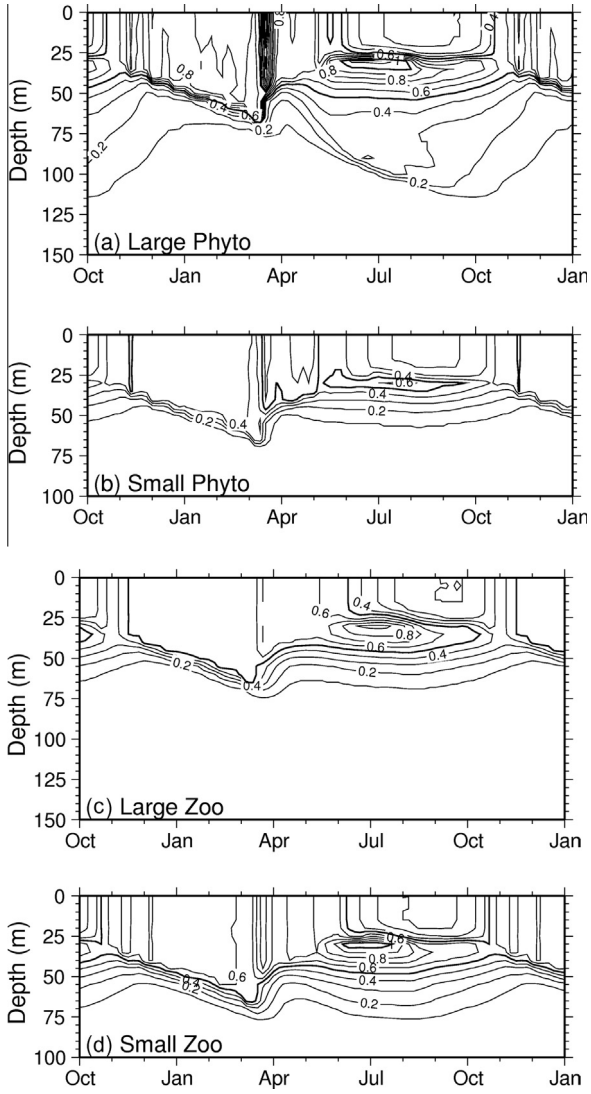

Fig. 3. Annual biomass (mmol N m^{-3}) distributions of (a) large phytoplankton, (b) small phytoplankton, (c) large zooplankton, (d) small zooplankton groups within the upper layer water column for the reference simulation ALBA1 (strong fish predation, strong upwelling, strong lateral nitrate input). The *x*-axis represents time with Day 1800 corresponds to the beginning of the model year at 1st October and day 2160 the end of September for the year that lasts for 360 days. The additional 90 days between 2160 and 2250 represent the autumn period of the subsequent year.

and summer. Both recycled nutrients as well as those supported from deeper levels by upwelling and laterally from the Gibraltar strait contribute to the subsurface production process.

The flagellate-based small cell group plays a less active role in this highly productive system. It contributes temporally to biomass production within the upper 40 m layer up to 0.4 mmol N m^{-3} during winter, followed by approximately 0.6 mmol N m^{-3} within the shallowing mixed layer under increasing light and temperature but decreasing nutrient conditions during April–May. A comparable level of production subsequently prevails within a thin layer of the seasonal thermocline during rest of the summer, below which relatively low water temperature and lack of light availability hamper their production.

The annual zooplankton biomass distribution closely follows that of the phytoplankton with an approximately 1-month time lag (Fig. 3c and d), consistent with the observations of Alcaraz et al. (2007). Because the large zooplankton group preys mainly on diatoms, its biomass reaches 0.5 mmol N m^{-3} during winter within the upper 50 m layer and 1.0 mmol N m^{-3} within subsurface levels during summer (Fig. 3c). The small zooplankton group also possesses a similar annual structure for both the surface and subsurface layers during the cold and warm periods, respectively (Fig. 3d).

The most notable feature of the annual nitrate distribution (Fig. 4a) is its absence within the surface layer for the entire year except for a limited period from the end of January to mid-March. The nitrate-deficient layer is connected to the subsurface nitrate pool across a very strong nitracline zone that typically varies up to 3–4 mmol N m^{-3} across a 5–10 m thick layer. A relatively high nitrate zone, greater than 5 mmol N m^{-3} (up to 8 mmol N m^{-3}), is identified below the nitracline. The nitracline layer follows the base of mixing layer remarkably well, as deduced from the distribution of vertical diffusivity in Fig. 2c. It also coincides with dense isolines of phytoplankton biomass along the base of the winter bloom layer and above the spring–summer subsurface high biomass layer (Fig. 3a and b). Those nutrients consumed above the nitracline represent new production, whereas those below this zone correspond to joint consequences of new and regenerated production, though regenerated production is the primary source.

In such a high input case, the amount of nitrate entering into the mixed layer in the winter is more than can be utilized by plankton production and thus accumulates up to 2 mmol N m^{-3} in February (Fig. 4a). It later leads to the intense March bloom once vertical mixing weakens considerably, as described above. The lack

of nutrients in the surface layer over the rest of the year implies their immediate utilization by plankton production once they enter into the surface layer either laterally or vertically. The entrainment process accounts for approximately 1 mmol N m^{-3} decrease below the base of mixing layer from its former values, >7 mmol N m^{-3} in autumn to <6 mmol N m^{-3} in the winter and early spring (Fig. 4a). Recalling that nitrate enters laterally into the water column within the 80 m upper layer, most of it accumulates within the subsurface levels without any involvement in the photic zone processes. In a stronger mixing case (due to more severe winter cooling and a sequence of winter storms), entrainment may be more active and may transfer more nutrients into the mixed layer, in which case there will be a further reduction in subsurface nitrate concentrations. This implies that the difference between nutrient concentration at 75–100 m depths during November and April may provide an indication of the severity of mixing and the level of entrainment in the NW Alboran Sea.

Further reduction of nitrate concentrations to approximately 5 mmol N m^{-3} in the spring signifies their consumption during the formation of the deep chlorophyll layer (Fig. 5a and b). This nitrate-based production is further supported by additional ammonium-based production due to its local recycling process at these depths (not shown). Once the spring–summer production weakens gradually and terminates by the end of summer, those that contributed to the production in the surface layer are deposited in the subsurface levels following the sinking and remineralization processes of particulate material. The subsurface nitrate concentration again exceeds 7 mmol N m^{-3} in autumn (Fig. 4a).

3.1.2. Moderately productive conditions

The previous simulation was repeated for the case of an order of magnitude lower lateral nitrate flux by Atlantic jet (ALBB1 in Table 4) as observed in the eastern part of the NW Alboran upwelling region. This case (Fig. 5a and b) differs from the reference simulation by the absence of an intense diatom bloom in March, indicating an important role of lateral enrichment in addition to the winter vertical mixing. The annual nitrate structure resembles the reference case, except with a slightly lower subsurface concentration (Fig. 4b). The annual structure of the large phytoplankton size group (Fig. 5a) closely resembles the one shown in Fig. 5a, but the small group (Fig. 5b) attains relatively low biomass over the year (<0.3 mmol N m^{-3}), except for a short-term spring peak of 0.5 mmol N m^{-3}. Given the strong predation pressure that is generally applicable for the NW Alboran Sea, we conclude that the simulations ALBA1 and ALBB1 represent the highly and moderately productive conditions, respectively.

The annual plankton structure in the Balearic Sea (Fig. 6) obtained from the simulation BAL1 (Table 4) differs from the standard simulation by the absence of the lateral nitrate influx, and the water column stratification presents a surface-intensified bloom of the large phytoplankton group from the beginning of December to the end of March, reaching a maximum phytoplankton biomass of 0.9 mmol N m^{-3} (Fig. 6a). The large phytoplankton group also contributes to the subsurface production over the depth of 100 m for the rest of the year. The contribution of the small phytoplankton group to the annual phytoplankton structure is limited to summer and is confined within the thermocline region (30–60 m) immediately below the surface mixed layer (Fig. 6b). The temperature limitation hinders its development in the relatively cold waters of approximately 13 °C below 50 m. The total zooplankton biomass (not shown) is generally dominated by large zooplankton group, which, however, does not exceed a biomass of 0.5 mmol N m^{-3}. This simulation represents a high phytoplankton - low zooplankton system in which the trophic flow is channelled through the large plankton food chain, and successfully reproduces the observed annual chlorophyll structure and water mass characteristics reported by Alcaraz et al. (2007).

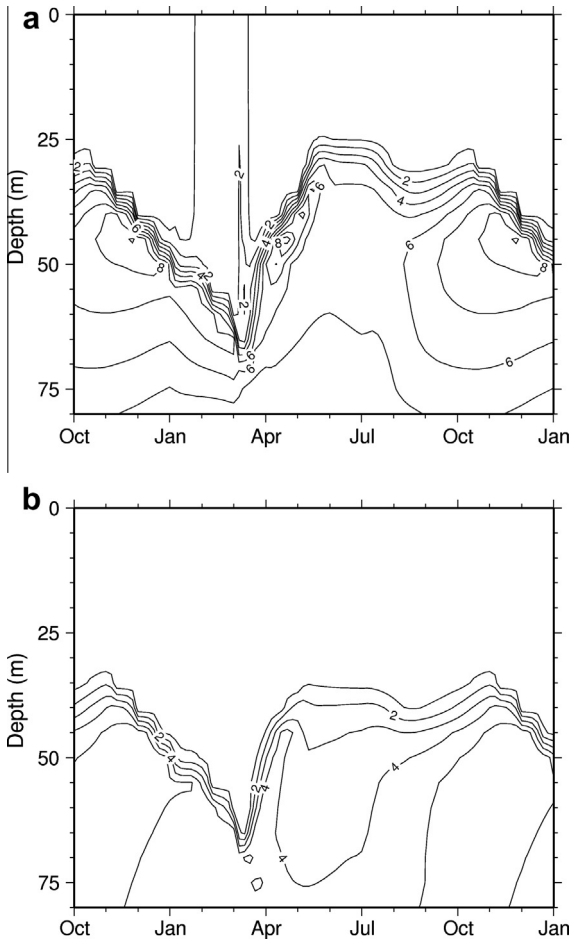

Fig. 4. Annual distributions of nitrate concentrations (mmol N m^{-3}) within the upper layer water column for the simulation (a) ALBA1 (strong fish predation, strong upwelling, strong lateral nitrate input), and (b) ALBB1 (strong fish predation, strong upwelling, weak lateral nitrate input).

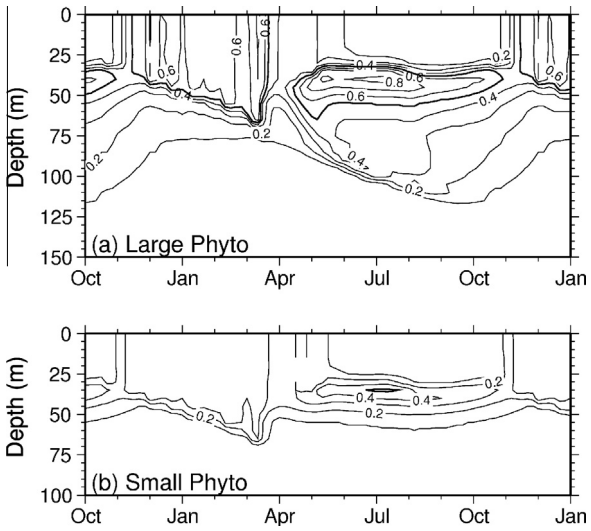

Fig. 5. Annual biomass (mmol N m^{-3}) distributions of (a) large phytoplankton group, (b) small phytoplankton group within the upper layer water column for the simulation ALBB1 (strong fish predation, strong upwelling, weak lateral nitrate input).

3.1.3. Oligotrophic conditions

The low productivity conditions observed within the Western anticyclonic Alboran gyre may be simulated by imposing a relatively weak lateral nitrate input, the downward vertical velocity of 0.5 m d^{-1} (instead of upwelling) and the absence of an outflowing nitrate flux (ALBE2 in Table 4). This simulation reveals winter diatom-based phytoplankton development with a maximum biomass level of 0.5 mmol N m^{-3} within the 50 m deep mixed layer in March (Fig. 7a). It attains only a limited extension of the subsurface layer in subsequent months, therefore giving rise to an oligotrophic system. No complementary summer production by flagellates takes place throughout the year due to severe nutrient limitation (Fig. 7b). The somewhat smaller lateral nitrate input and/or stronger downwelling velocity may further reduce phytoplankton biomass and shift the system towards more oligotrophic conditions as observed in the Algerian basin.

3.2. Response of annual plankton structure to the zooplankton grazing and fish predation formulations

3.2.1. Zooplankton grazing formulation

The present work parameterizes the food preferences of zooplankton groups in terms of the relative proportion of the total food available in the system (see Eq. (A5a,b)). This approach allows optimum zooplankton feeding by automatic switching between prey items depending on their relative abundance. An alternative approach is to set the food preference coefficients to constant values that apply for all seasons and over the water column. Here, we show how the use of the latter approach may lead to an erroneous annual plankton structure when used with the current parameter setting of the model.

For example, the simulation ALBA1c (Table 4) with constant food preference coefficients delineates only minor differences in phytoplankton biomass changes as shown by comparing Fig. 8 with the reference simulation shown in Fig. 3, This choice of constant coefficients results in slightly higher (approximately 0.2 mmol N m^{-3}) biomass distributions throughout the year. Another case (the simulation ALBB3c in Table 4) that also employs constant coefficients gives rise to a substantially different food

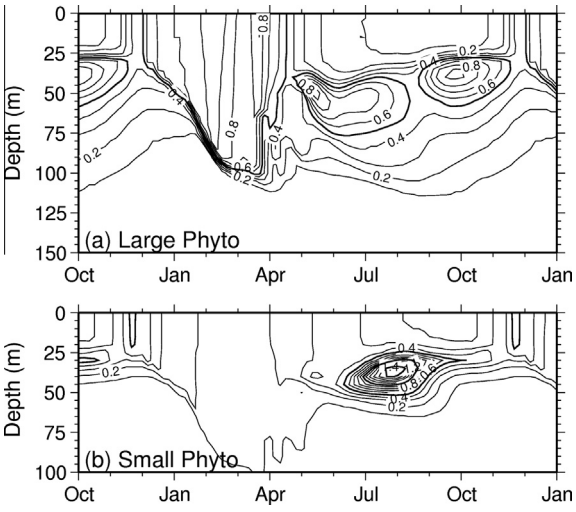

Fig. 6. Annual biomass (mmol N m^{-3}) distributions of (a) large phytoplankton group, and (b) small phytoplankton group within the upper layer water column for the simulation BAL1 (strong predation rate, strong upwelling). Day 2880 corresponds to 1st October and the year lasts for 360 days at 3240. The additional 90 days between 3240 and 3330 represent the autumn period of the subsequent year.

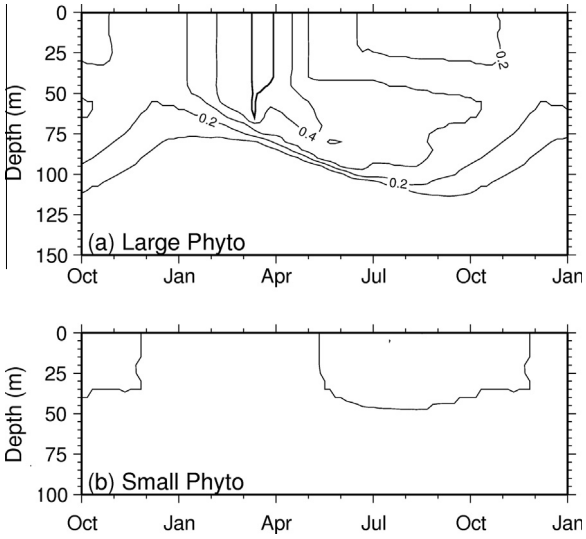

Fig. 7. Annual biomass (mmol N m^{-3}) distributions of (a) large phytoplankton group, (b) small phytoplankton group within the upper layer water column for the simulation ALBE2 (weak fish predation, intermediate downwelling, weak lateral nitrate input).

web structure. It is dominated by the small phytoplankton and large zooplankton groups with their very high biomass and negligible biomass of the large phytoplankton and small zooplankton groups, even if this case applies to the moderately productive conditions with relatively low lateral nitrate input compared to the simulation ALBA1c (Fig. 9). However, the same simulation provides a more balanced biomass structure of plankton groups with lower values in the case of using variable coefficients (the simulation ALBB3 in Table 4) (not shown).

When defining constant food preference coefficients, the development of realistic or spurious annual plankton structures appears to depend on the choice of the fish predation rate constant. The choice of a relatively strong predation pressure (ALBA1c case) apparently provides a balanced system of top-down and bottom-up controls that prevents the competitive exclusion of a particular plankton group from the system. In the case of weaker predation pressure (ALBB3c case), this balance is disturbed in favor of excessive mesozooplankton growth. The dominant mesozooplankton group then continuously and heavily (due to the choices of constant food preferences) predates on the large phytoplankton and microzooplankton groups and thus leads to their exclusion from the community structure. The lack of microzooplankton grazing pressure together with relatively low food preference of mesozooplankton allow the small phytoplankton group to grow more freely without a major predation pressure and so dominate the annual phytoplankton biomass. In contrast, in the case of alternative food-dependent parameterization, the relatively high food preference of mesozooplankton on decreasing large phytoplankton biomass and low food preference on increasing small phytoplankton biomass compensate each other and accounts for the fairly similar food shares in terms of the total available food and therefore lead to a more balanced combination of large and small size plankton groups (coexistence).

3.2.2. Fish predation formulation

Recalling likely role of fish predation pressure on the development of spurious solutions, we next examined whether its biomass-dependent specification may circumvent this ambiguity even in the case of constant food preferences. Defining the biomass dependence by a hyperbolic function, the new predation rate f_{0k} is expressed by

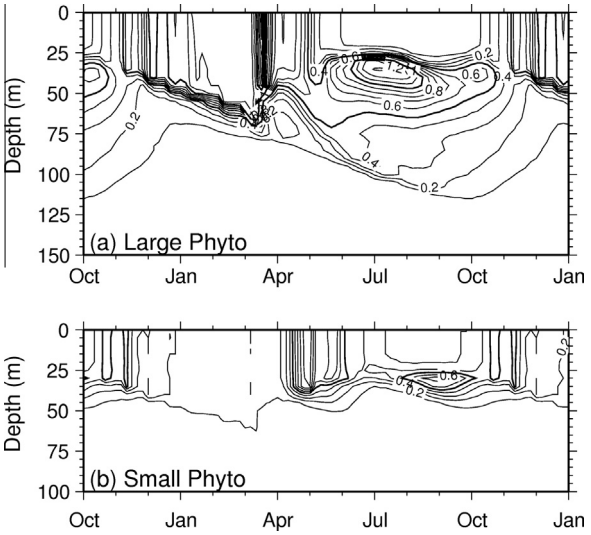

Fig. 8. Annual biomass (mmol N m^{-3}) distributions of (a) large phytoplankton group, (b) small phytoplankton group within the upper layer water column for the reference simulation ALBA1c using constant food preference coefficients.

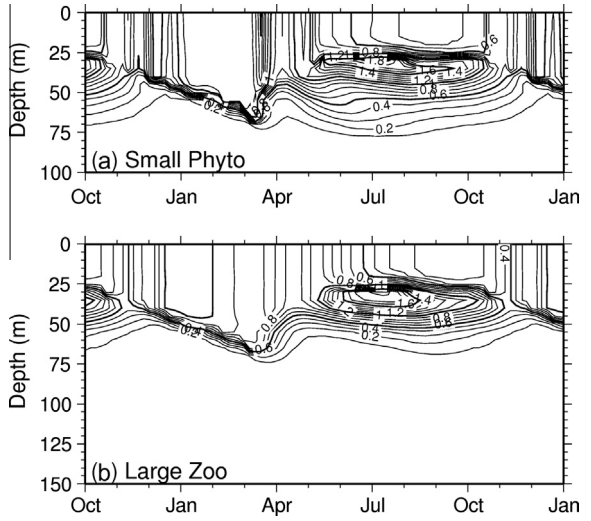

Fig. 9. Annual biomass (mmol N m^{-3}) distributions of (a) small phytoplankton group, (b) large zooplankton group within the upper layer water column for the simulation ALBB3c using constant food preference coefficients.

$$f_{0k}(Z) = f_{1k}(Z_k/(K_{Fk} + Z_k)) \quad (3)$$

where f_{1k} denotes a constant rate parameter and K_{Fk} is the half saturation constant of the food dependence for each zooplankton group. In the new parameterization, f_{0k} approaches f_{1k} at a relatively high zooplankton biomass (depending on the choice of K_{Fk}), but attains lower values at low zooplankton biomass of weakly productive conditions. Thus, this representation makes the predation rate relatively strong for productive regions and weak for less productive regions, as expected. This is conceptually similar to the specification of biomass dependent food preference coefficients. The simulation ALBB3, which includes constant food preferences (the unbalanced simulation described above), repeated with this revised fish predation parameterization is able to provide a more reasonable phytoplankton biomass distribution (not shown). Furthermore, setting $f_{1k} * Z_k = f_{2k} \approx$ constant in Eq. (3), the quadratic predation functional form used in Eqs. (A4a) and (A4b) reduces to the hyperbolic functional form that has been used as the closure term in some ecosystem models (e.g., Fasham, 1993; Martin et al., 2001; Gentleman et al., 2003; Mitra, 2009). Our various test simulations with the hyperbolic closure also showed similarly improved performance.

4. Discussion

The present study documents a one-dimensional physical–biochemical modeling system for the Alboran and Balearic Sea ecosystems and illustrates its capability to simulate different biological characteristics and peculiarities extending from highly productive upwelling systems to oligotrophic gyres. A physical model that simultaneously computes temporal variations of temperature, salinity and vertical diffusivity over the water column complements the biological model. This intermediate complexity N2P2Z2D-type biochemical model is considered the minimal configuration necessary to adequately reproduce the primary observed features of the region. Introducing additional complexity is not foreseen as a reasonable step prior to fully exploring its three-dimensional capability when simulating physically driven features of the region. The level of model complexity may be considered sufficient provided that exploration of complex biological issues such as changes in biodiversity, ecosystems functioning and their services are beyond the scope of our present interest. Such studies may indeed require more sophisticated formulations of the microbial loop and coupling between the higher and lower trophic levels. A particular limitation is the lack of sufficient data with better temporal and spatial coverages that, if available, would support the empirical basis for testing and validating and more rigorously evaluating this relatively simple complexity model (in terms of its rates, grazing, and loss terms) when applied to different locations. The data availability for model validation is, however, a general chronic problem of the marine ecosystem modeling.

The model simulations point to the importance of specifying biomass dependence for the food preference coefficients in terms of the relative proportion of total food and the predation pressure coefficients using a hyperbolic (or sigmoidal) function of zooplankton biomass. Both of them adjust their values depending on the availability of biomass during the year and within the water column. Instead, keeping them constant for all conditions (i.e., no switch between prey types) makes the trophic links between the food web components too rigid to be adapted to internal dynamic conditions. As a result, the system may develop a spurious dynamical equilibrium. As a matter of fact, following Gentleman et al. (2003), there is a growing awareness of the impact of the choice of grazing formulation on the resulting food web structure (Anderson et al., 2010; Prowe et al., 2012). Considerable differences are noted in the phytoplankton distributions of North Atlantic and North Pacific depending on the functional form of the zooplankton grazing (Anderson et al., 2010). Moreover, whatever the choice of its functional form, active switching has been shown to promote coexistence by damping the changes in individual phytoplankton biomass, whereas the no switching case amplifies changes in phytoplankton biomass and thus may promote the dominance of individual phytoplankton types (Prowe et al., 2012). Our simulations with no-switch and active-switch choices nicely demonstrate these alternatives and provide strong support for a key role of the grazing formulation on annual plankton succession and community structure. This particularly applies in the case of weak fish predation pressures and relatively strong prey choice, which reduces the critical importance for the choices of no-switch and active-switch preference on the zooplankton grazing formulation. The choice of the Holling Type II (i.e., hyperbolic) functional form of the fish predation and active switching appears to work well for the Alboran and Balearic Seas, irrespective of the intensity of bottom-up resource control on the plankton production.

Consistent with the available observations, the annual phytoplankton structure comprises a surface-intensified biomass development within a relatively deep mixed layer (~60 m) from mid-November to early spring. This is initiated by new production and later complemented by regenerated production and is mostly contributed by the large size group. It is followed by the equally strong plankton production within the deep chlorophyll maximum layer during rest of the year, generally contributed by both groups at almost equal proportions. The presence of relatively strong stratification in the NW Alboran Sea limits the efficiency of nitrate entrainment from subsurface levels, but this deficiency is compensated by the persistent lateral supply. Moderately and highly productive systems of the Alboran Sea may always produce sufficient zooplankton biomass to sustain relatively high fishery because its relatively simple ecosystem structure channels the trophic flow efficiently into fish production, whereas the other surrounding seas, such as the Black Sea, the Adriatic Sea, and the Baltic Sea divert a considerable part of the trophic flow to the dead-end jelly-dominated food web (see e.g., Oguz et al., 2008). We think that this feature may contribute to an explanation of the "paradox of the Mediterranean", which implies high fishery yield under relatively low primary production (Alcaraz et al., 1994; Estrada, 1996).

Assuming that 1 mmol N m^{-3} biomass roughly equals 2 mg m^{-3} chlorophyll, the biomass range of 1.0–1.5 mmol N m^{-3} provided by the model simulations for the intense upwelling/lateral nitrate inflow case agrees with the empirical data. Having the subsurface total biomass in the range of 1.0–1.5 N m^{-3} is again consistent with spring–summer deep chlorophyll maxima observations. The presence of a nitrate accumulation layer simulated by the model that roughly coincides with the deep chlorophyll maximum layer in spring–summer months has not been emphasized before, but its observational evidence may be traced by the available measurements (Ramírez et al., 2005; Macías et al., 2011). This layer may be used as an indicator of the level of enrichment by the Atlantic jet. Moreover, the difference between the relatively high nitrate concentrations in the autumn prior to winter mixing with respect to relatively lower values in spring may serve as an indicator for the severity of winter bloom in general and the dense March bloom in particular. The nitracline layer that is sequeezed between the upwelled and vertically mixed nitrate structures from deeper parts of the water column and surface layer, respectively, emerges as another characteristic feature of the upwelling systems of the region. This layer also coincides with the closely packed isolines of phytoplankton biomass below the mixed layer in autumn-winter and above the DCM in spring–summer. Capturing the nitracline zone and resolving the nitrate accumulation layer properly by observations may be critical to inferring many features of the system. However, this requires high-resolution sampling, preferably not more than 3–5 m, between the 50–100 m depth range.

The capability of the model to simulate different regional ecosystem conditions indicates its further use as a tool to evaluate different aspects of the regional ecosystem characteristics, elaborate specific processes deduced from field measurements, investigate the long-term interannual variability, etc. It may be easily configured for different physical systems by defining the magnitude of upwelling/downwelling velocity and lateral nitrate influx/outflux (for setting up the regional physical conditions), the appropriate water column temperature, salinity and nitrate profiles (for the initial conditions), and the daily variations of sea surface temperature, salinity, photosynthetically available radiation (for the surface boundary conditions).

The significance of climate dependence of plankton production characteristics in the region was recently raised by increasing contributions of coccolithophores and dinoflagellates by the end of 1990s (Mercado et al., 2007). This trend is consistent with the progressive reduction of the upwelling intensity, the larval growth of *Sardine pilchardus* and their nutritional condition (Mercado et al., 2007). Therefore, one novel subject that may be considered for a future study concerns the direct and indirect impacts of climate variability (Fernandez de Puelles and Molinero, 2008; Calvo et al., 2011; Mercado et al., 2012). Studying its indirect impact is relatively straightforward and requires forcing the physical model with appropriate long-term meteorological conditions. For warm years, the model is expected to produce less efficient vertical turbulent mixing and thus weaker nutrient entrainment as well as a subsequent weaker winter and early spring plankton production, and vice-versa for cold years. The present model is set preferentially for moderately productive winter climatic conditions. Modeling direct effects of climate changes is more challenging and requires a reasonably accurate formulation of the temperature dependence of growth and mortality processes. Otherwise, phenological changes on the plankton groups cannot be modeled realistically. In its three-dimensional context, another potentially important subject of a future study is to elaborate relative roles of the large and mesoscale features of the regional plankton productivity.

5. Conclusions

A one-dimensional coupled physical-biochemical model was implemented for the Alboran and Balearic Sea ecosystems that (i) extends the previous single-compartment plankton models to the double-compartmental case and therefore distinguishes between mesotrophic and oligotrophic conditions and reproduce the deep chlorophyll maximum layer structure more realistically, (ii) provides a systematic assessment for the relative roles of bottom-up and top-down controls in different ecological conditions, (iii) incorporates explicit parameterizations of the vertical and horizontal advective nutrient fluxes in a one-dimensional modeling context, which is generally missing in majority of the one-dimensional models, (iv) enables the reproduction of different ecological conditions of the Alboran and Balearic Seas by altering the upwelling velocity and vertical and horizontal nitrate fluxes, thereby demonstrating the sensitivity of regional food web structures to the regional physical conditions, (v) shows sensitivity of the lower trophic food web structure to different forms of the zooplankton grazing parameterization, in other words, importance of the choice of the zooplankton grazing parameterization for a realistic representation of the annual plankton structure, and (vi) illustrates development of spurious lower trophic level food web structures for some range of values of the fish predation rate and explains how to avoid such spurious solutions.

Acknowledgements

The present work is a contribution to the EU 7th Framework project called "Perseus (Policy-oriented marine environmental research for the Southern European Seas)". The authors thank the reviewers for their useful comments on the earlier version of the manuscript. D.M. was supported by a JaeDOC contract (#X0SC000087) of the Spanish Council for Scientific Research (CSIC). Additional support was provided by the Spanish National Research Project CTM2011-22580.

Appendix A. Biological model equations

A.1. Phytoplankton dynamics

Temporal variations of the large (P_L) and small (P_S) phytoplankton biomass are governed by the biological source-sink terms of the form

$$R_{PX} = \sigma_X \cdot f_X(N,A) \cdot f_X(I) \cdot f_X(T) \cdot P_X - \sum G(P_X) \cdot Z_X - m_{PX} \cdot P_X \quad \text{(A1)}$$

where the subscript X denote either L for large phytoplankton or S for small phytoplankton size group. The right hand side describes, respectively, the phytoplankton growth (primary production), grazing by zooplankton, and physiological mortality that also includes the respiration. This simplification is justified in the absence of explicit representation of the microbial loop.

The phytoplankton growth is modeled as the products of maximum specific growth rate σ, phytoplankton bimass P, simultaneous limitations by the availability of nitrogen resource f(N,A), photosythetically available radiation f(I), and temperature f(T). The light limitation is parameterized by (Jassby and Platt, 1976)

$$f_X(I) = \tanh[\alpha_X \cdot I] \quad \text{with} \quad I = I_S \cdot \exp\left(-\int_0^z k \cdot dz\right) \quad \text{(A2)}$$

where α is a parameter controlling slope of the light limitation curve at low values of the photosynthetically available irradiance (PAR) whose surface intensity I_S amounts to half of the incoming solar radiation. Its attenuation below the sea surface is represented by an exponential decay function (Eq. A2) in which the total extinction coefficient k comprises the contributions from sea water itself (k_w), and self-shading effects of phytoplankton and detritus material (k_b); $k = k_w + (P_L + P_S + D)k_b$.

The nitrogen limitation function comprises the sum of individual contributions of the ammonium and nitrate limitations; $f_X(N,A) = f_X(N) + f_X(A)$. They are expressed by the Monod-type hyperbolic functions involving a saturation response at high resource concentrations

$$f_X(A) = \left[\frac{A}{K_{AX} + A}\right] \quad \text{(A3a)}$$

$$f_X(N) = \left[\frac{N}{K_{NX} + N}\right] \cdot \left[\frac{K_{AX}}{K_{AX} + A}\right] \quad \text{(A3b)}$$

where A and N denote ammonium and nitrate concentrations, respectively; K_{AX} and K_{NX} are the corresponding half saturation constants of ammonium and nitrate uptakes, and the subscript X denotes either large or small phytoplankton group. The term within the second square brackets of Eq. (A3b) represents ammonium limitation of the nitrate uptake due to preferred consumption of ammonium with respect to nitrate in the growth process. The silicate control on the diatom growth is neglected because no evidence exists for the prevailing role of this process for this region. The temperature control of the phytoplankton growth is parameterized by

$$f_X(T) = Q_{10,X}^{(T-20)/10} \quad \text{(A3c)}$$

where Q_{10} is a constant parameter, and T denotes temperature. According to Eq. (A3c), the temperature limitation becomes more effective at decreasing temperatures below 20 °C. The value of $f(T)$ is set to unity for $T > 20$ °C.

A.2. Zooplankton dynamics

Changes in the microzooplankton (Z_S) and mesozooplankton (Z_L) biomass are controlled by ingestion, predation, mortality and excretion which are expressed by

$$R_{ZS} = \gamma_s \cdot [G_{ZS}(P_S) + G_{ZS}(P_L) + G_{ZS}(D)] \cdot Z_S - G_{ZL}(Z_S) \cdot Z_L - \mu_S \cdot Z_s - m_{ZS} \cdot Z_s - f_P Z_S^2 \quad \text{(A4a)}$$

$$R_{ZL} = \gamma_L \cdot [G_{ZL}(P_S) + G_{ZL}(P_L) + G_{ZL}(D) + G_{ZL}(Z_s)] \cdot Z_L - \mu_L \cdot Z_L - m_{ZL} \cdot Z_L - f_P Z_L^2 \quad \text{(A4b)}$$

where γ_X, μ_X and m_{ZX} are, respectively, the assimilation coefficient, excretion rate and mortality rate with the subscript X denoting either L for large zooplankton or S for small zooplankton size group. The terms expressed in the quadratic form parameterize the grazing pressure of higher predators with a constant predation rate f_P (Steele and Henderson, 1992). They are a complete lost from the system without any recycling. The ingestion terms are represented by the Michaelis–Menten functional form and consider food preferences on diatoms, flagellates, and detritus. The food preference coefficients of zooplankton are expressed as a function of the relative proportion of the total food (Vanderploeg and Scavia, 1979; Fasham et al., 1990; Gentleman et al., 2003) by

$$a_j = \frac{a_j^* X_j}{Food_L} \quad b_j = \frac{b_j^* Y_j}{Food_S} \quad \text{(A5a, b)}$$

where a_j^* and b_j^* represent the constant food preference coefficients, X_j and Y_j are food items for the large and small zooplankton groups, and $Food_k$ defines the total food available for each zooplankton group expressed by

$$Food_L = a_L P_L + a_S P_S + a_D D + a_Z Z_{ZS} \quad \text{and}$$
$$Food_S = b_L P_L + b_S P_S + b_D D \quad \text{(A5c, d)}$$

According to (A5a,b), when a food type declines, its grazing preference decreases. In this case, an alternative food type having higher biomass is selected by zooplankton. For example, the ingestions of micro- and mesozooplankton on flagellates are defined, respectively, by

$$G_{ZS}(P_S) = g_S \cdot \frac{b_S P_S}{K_{ZS} + Food_S} \quad \text{and}$$
$$G_{ZL}(P_S) = g_L \cdot \frac{a_S P_S}{K_{ZL} + Food_L} \quad \text{(A6a, b)}$$

where g_S and g_L denote the maximum specific grazing rates for micro- and mesozooplankton groups, respectively, and K_{ZS}, K_{ZL} are the corresponding half saturation constants of zooplankton ingestions. Similar expressions are applied for the grazing of diatoms and detritus by both zooplankton groups and grazing of the microzooplankton group by mesozooplankton.

A.3. Nutrient recycling processes

Fecal pellets (unassimilated part of the food grazed) and phytoplankton and zooplankton mortalities form the sources for the detritus compartment of the model. Its transformation into ammonium at a rate ε_D constitutes a sink of detritus in addition to its settling by zooplankton groups within the water column. The source-sink terms for the detritus equation then read

$$R_D = (1-\gamma_s) \cdot [G_{ZS}(P_S) + G_{ZS}(P_L)] \cdot Z_S + m_S \cdot P_S + m_L \cdot P_L + m_S \cdot Z_S + m_L \cdot Z_L + (1-\gamma_L) \cdot [G_{ZL}(P_S) + G_{ZL}(P_L) + G_{ZL}(Z_S)] \cdot Z_L - \gamma_s \cdot G_{ZS}(D) - \gamma_L \cdot G_{ZL}(D) - \varepsilon \cdot D \quad \text{(A7)}$$

The model considers, for simplicity, only one class of detritus particles produced by all phytoplankton and zooplankton groups. They sink with the single settling velocity w_D that depends on the concentration by

$$w_D = w_{D,\max} \frac{D}{K_D + D} \quad \text{(A8)}$$

where $w_{D,max}$ is the maximum sinking speed at high detritus concentrations and/or when small particles are aggregated in the form of large particles. This approach may be considered as a simplified version of assigning two different size classes of detritus produced separately from two different plankton food chains and sinking

with different settling speeds in the model. A similar functional form is used for sinking of diatoms.

Excretion by two zooplankton groups and remineralization of detritus provide the supply of recycled ammonium concentration. The losses are ammonium uptake during phytoplankton production and its oxidation to nitrate. They are expressed by

$$R_A = -[\sigma_S \cdot f_S(A) \cdot f_S(I) \cdot f_S(T) \cdot P_S + \sigma_L \cdot f_L(A) \cdot f_L(I) \cdot f_L(T) \cdot P_L] - r \cdot A + \varepsilon \cdot D + \mu_S \cdot Z_s + \mu_L \cdot Z_L \quad (A9)$$

The source-sink terms of nitrate equation consists of a source from ammonium oxidation (i.e. nitrification) and a loss by nitrate uptake, as given by

$$R_N = -[\sigma_S \cdot f_S(N) \cdot f_S(I) \cdot f_S(T) \cdot P_S + \sigma_L \cdot f_L(N) \cdot f_L(I) \cdot f_L(T) \cdot P_L] + r \cdot A \quad (A10)$$

The nitrification rate is made light (and thus depth) dependent according to

$$r = r_{\max} \frac{K_{PAR}}{K_{PAR} + I} \quad (A11)$$

where $r_{\max}$ is the maximum nitrification rate, I denotes the photosynthetically available radiation within the water column, and K_{PAR} is the half saturation constant regulating the intensity of nitrification according to the available radiation. According to Eq. (A11), the nitrification rate vanishes at high light intensity near the surface but increases toward the base of euphotic layer and the nitracline zone as the light intensity tends to zero.

A.4. Boundary and initial conditions, numerical procedure

All vertical diffusive and advective fluxes are set to zero at the surface and bottom boundaries of the biological model. Thus, for any state variable F, we take

$$(K_h \frac{\partial F}{\partial z}) = 0 \quad \text{and} \quad w \cdot F = 0 \text{ at } z = 0 \quad \text{and} \quad z = -h \quad (A12)$$

They are complemented by specification of the upwelling flux of nitrate ($w \cdot N_b$) and the absence of sinking flux of detritus at the bottom boundary

$$w_D \frac{\partial D}{\partial z} = 0 \quad \text{at } z = -h \quad (A13)$$

The biological model (Eqs. (A1)–(11)) together with the boundary conditions (Eqs. (A12) and (A13)) form a fully conservative system except predation losses of zooplankton and provided that any fecal pellet loss is compensated by the upward flux of nitrate at the bottom boundary. In the present model, we locate the bottom boundary well below the level of active remineralization zone. This choice together with a relatively low settling speed (less than its maximum value of 8.0 m d^{-1}) allow a complete remineralization of the detrital pool within the water column without appreciable export flux of particulate matter from the system. This setting therefore avoids dealing with a time-dependent nitrate-based flux prescription at the lower boundary of the model to compensate the detritus loss.

The biochemical model is initialized by an idealized vertical nitrate structure. Other state variables of the biochemical model are initialized by small positive constant values to allow positive growth and utilization over the water column. The coupled model is integrated for eight years to achieve a yearly perpetual cycle of the upper layer physical and biological structures. Typically, the equilibrium states of the biological and physical variables are established after four years of the transient adjustment period. A time step of 10 min is used for the numerical integration of the system of equations.

A.5. Choices of the parameter values

The smaller size phytoplankton group is made better adapted to the low nutrient–high light and high temperature conditions whereas the larger size group to high nutrient–low light and relatively low temperature conditions. This is achieved by assigning (1) a relatively larger maximum growth rate (2.8 d^{-1} at $T \geqslant 20$ °C) for the microphytoplankton group with respect to relatively low rate of 2.2 d^{-1} for nanophytoplankton; (2) a relatively high value for the initial slope of light limitation curve for the large group with respect to the small group (α_L = 0.32 W^{-1} m^2; α_S = 0.30 W^{-1} m^2) (Moran and Estrada, 2001); (3) relatively low half saturation constants of nitrate and ammonium uptakes for small phytoplankton group that make it more proficient at utilizing low levels of nutrients (K_{NL} = 0.5, K_{NS} = 0.3 mmol N m^{-3} and K_{AL} = 0.5, K_{AS} = 0.3 mmol N m^{-3}) where lower values of the ammonium half saturation constants with respect to nitrate reflect a general preference of ammonium uptake first; and (4) setting a higher value for Q_{10} parameter for the small size group making its growth more favourable at higher temperatures (Q_{10L} = 1.5, Q_{10S} = 2.0). Moreover, mortality of both phytoplankton groups is taken to be a constant fraction of their standing biomass and is assumed to be higher for the smaller size group (m_{PL} = 0.04 and m_{PS} = 0.06 d^{-1}). The large phytoplankton group is considered to sink with a maximum speed of 2.0 m d^{-1}. The available bio-optical measurements yield the thickness of the euphotic zone on the order of 100 m, implying the overall attenuation coefficient of PAR in the range of roughly k = 0.05–0.06 m^{-1} (e.g. Moran and Estrada, 2001; Mercado et al., 2006). In consistent with these findings, we set k_w = 0.05 m^{-1} and k_b = 0.02 m^{-1} (mmol m^{-3})$^{-1}$.

Microzooplankton are assumed to graze on small phytoplankton with a greater efficiency ($b_S^* = 0.6$) than on large phytoplankton ($b_L^* = 0.3$) and detritus ($b_D^* = 0.2$). Mesozooplankton are considered to have a more diverse diet expressed by a decreasing order of food capture efficiency values; $a_L^* = 0.7$ for large phytoplankton, $a_Z^* = 0.4$ for microzooplankton, $a_D^* = 0.3$ for detritus, and $a_S^* = 0.2$ for small phytoplankton. Thus, microzooplankton and detritus may constitute their alternative diet in the absence of phytoplankton. We note that these food preference coefficients are not directly used in the grazing formulations, but they are modified according to Eq. (A5a,b). Microzooplankton acquires a higher maximum grazing rate (g_S = 1.0 d^{-1}) as compared to that of mesozooplankton (g_L = 0.7 d^{-1}). Microzooplankton grazing responds more rapidly to increase in phytoplankton biomass than mesozooplankton; thus we set K_{ZS} = 0.7, K_{ZL} = 0.9 mmol N m^{-3}. The microzooplankton have also higher excretion rate and the food assimilation efficiency; μ_S = 0.09 d^{-1}; and γ_S = 0.8. The corresponding values for the mesozooplankton group are μ_L = 0.05 and γ_L = 0.7. The model specifies a constant fish predation pressure rate of f_P = 0.15 (mmol N)$^{-1}$ m^3 d^{-1} for both zooplankton groups as a representative of the entire higher trophic level. This estimate is obtained by assuming the fish-induced predation mortality rate of about 0.008–0.015 d^{-1} (Travers and Shin, 2010), and a typical fish biomass of about 0.1 mmol N m^{-3}.

Appendix B. Supplementary material

Supplementary data associated with this article can be found, in the online version, at http://dx.doi.org/10.1016/j.pocean.2013.03.001.

References

Alcaraz, M., Saiz, E., Estrada, M., 1994. Excretion of ammonia by zooplankton and its potential contribution to nitrogen requirements for primary production in the Catalan Sea (NW Mediterranean). Marine Biology 119, 69–76.

Alcaraz, M., Calbet, A., Estrada, M., Marrasé, C., Saiz, E., Trepat, I., 2007. Physical control of zooplankton communities in the Catalan Sea. Progress in Oceanography 74, 294–312.

Anderson, T.R., Gentleman, W.C., Sinha, B., 2010. Influence of grazing formulations on the emergent properties of a complex ecosystem model in a global ocean general circulation model. Progress in Oceanography 87, 201–213.

Bahamón, N., Cruzado, A., 2003. Modelling nitrogen fluxes in oligotrophic environments: NW Mediterranean and NE Atlantic. Ecological Modelling 163, 223–244.

Bakun, A., Agostini, V.N., 2001. Seasonal patterns of wind induced upwelling/downwelling in the Mediterranean Sea. Scienta Marina 65, 243–257.

Barale, V., Jaquet, J.M., Ndiaye, M., 2008. Algal blooming patterns and anomalies in the Mediterranean Sea as derived from the SeaWiFS data set (1998–2003). Remote Sensing of Environment 112, 3300–3313.

Bellido, J.M., Brown, A.M., Valavanis, V.D., Giraldez, A., Pierce, G.J., Iglesias, M., Palialexis, A., 2008. Identifying essential fish habitat for small pelagic species in Spanish Mediterranean waters. Hydrobiologia 612, 171–184.

Bissinger, J.E., Montagnes, D.J.S., Sharples, J., Atkinson, D., 2008. Predicting marine phytoplankton maximum growth rates from temperature: improving on the Eppley curve using quantile regression. Limnology and Oceanography 53 (2), 487–493.

Bosc, E., Bricaud, A., Antoine, D., 2004. Seasonal and interannual variability in algal biomass and primary production in the Mediterranean Sea, as derived from four years of SeaWiFS observations. Global Biogeochemical Cycles 18, GB1005.

Calvo, E., Simó, R., Coma, R., Ribes, M., Pascual, J., Sabatés, A., Gili, J.M., Pelejero, C., 2011. Effects of climate change on Mediterranean marine ecosystems: the case of the Catalan Sea. Climate Research 50, 1–29.

Coll, M. et al., 2011. The Mediterranean Sea under siege: spatial overlap between marine biodiversity, cumulative threats and marine reserves. Global Ecology and Biogeography. http://dx.doi.org/10.1111/j.1466-8238.2011.00697.x.

D'Ortenzio, F., D'Alcala, M.R., 2009. On the trophic regimes of the Mediterranean Sea: a satellite analysis. Biogeoscience 6 (2), 139–148.

Dafner, E.V., Boscolo, R., Bryden, H.L., 2003. The N:Si:P molar ratio in the Strait of Gibraltar. Geophysical Research Letters 30 (10), 13.1–13.4.

Denman, K.L., 2003. Modelling planktonic ecosystems: parameterizing complexity. Progress in Oceanography 57, 429–452.

Ducklow, H.W., Fasham, M.J.R., 1992. Bacteria in the greenhouse: modeling the role of oceanic plankton in the global carbon cycle. In: Mitchell, R. (Ed.), Environmental Microbiology. Wiley-Liss, New York, pp. 1–32.

Estrada, M., 1996. Primary production in the northwestern Mediterranean. Scientia Marina 60, 55–64.

Estrada, M., Marrase, C., Latasa, M., Berdalet, E., Delgado, M., Riera, T., 1993. Variability of the Deep Chlorophyll Maximum characteristics in the northwestern Mediterranean. Marine Ecology Progress Series 92 (3), 289–300.

Fasham, M.J.R., 1993. Modelling the marine biota. In: Heimann, M. (Ed.), The Global Carbon Cycle. Springer-Verlag, Berlin, pp. 457–504.

Fasham, M.J.R., Ducklow, H.W., McKelvie, S.M., 1990. A nitrogen-based model of plankton dynamics in the oceanic mixed layer. Journal of Marine Research 48, 591–639.

Fernandez de Puelles, M.L., Molinero, J.C., 2008. Decadal changes in hydrographic and ecological time-series in the Balearic Sea (western Mediterranean), identifying links between climate and zooplankton. ICES Journal of Marine Science 65, 311–317.

García, A., Cortés, D., Ramirez, T., Giráldez, A., Carpena, A., 2003. Contribution of larval growth rate variability to the recruitment of the Bay of Malaga anchovy (SW Mediterranean) during the 2000–2001 spawning seasons. Scientia Marina 67, 477–490.

García-Gorriz, E., Carr, M.-E., 1999. The climatological annual cycle of satellite-derived phytoplankton pigments in the Alboran Sea. Geophysical Research Letters 26 (19), 2985–2988.

García-Lafuente, J., Cano, N., Vargas, M., Rubín, J.P., Hernandez-Guerra, A., 1998. Evolution of the Alboran Sea hydrographic structures during July 1993. Deep Sea Research I 45, 39–65.

Gentleman, W., Leising, A., Frost, B., Strom, S., Murray, J., 2003. Functional responses for zooplankton feeding on multiple resources: a review of assumptions and biological dynamics. Deep-Sea Research II 50, 2847–2875.

Gibson, G.A., Spitz, Y.H., 2011. Impacts of biological parameterization, initial conditions, and environmental forcing on parameter sensitivity and uncertainty in a marine ecosystem model for the Bering Sea. Journal of Marine Systems 88, 214–231.

Gibson, G.A., Musgrave, D.L., Hinckley, S., 2005. Non-linear dynamics of a pelagic ecosystem model with multiple predator and prey types. Journal of Plankton Research 27 (5), 427–447.

Jassby, A.D., Platt, R., 1976. Mathematical formulation of the relationship between photosynthesis and light for phytoplankton. Limnology and Oceanography 21, 540–547.

Kone, V., Machu, E., Penven, P., Andersen, V., Garçon, V., Freon, P., Demarcq, H., 2005. Modeling the primary and secondary productions of the southern Benguela upwelling system: a comparative study through two biogeochemical models. Global Biochemical Cycles 19, GB4021.

Latasa, H., Estrada, M., Delgado, M., 1992. Plankton-pigment relationships in the Northwestern Mediterranean during stratification. Marine Ecology Progress Series 88, 61–73.

Lima, I.D., Olson, D.B., Doney, S.C., 2002. Intrinsic dynamics and stability properties of size-structured pelagic ecosystem models. Journal of Plankton Research 24, 533–556.

Macias, D., Navarro, G., Echevarria, F., Garcia, C.M., Cueto, J.L., 2007. Phytoplankton pigment distribution in the northwestern Alboran Sea and meteorological forcing: a remote sensing study. Journal of Marine Research 65, 523–543.

Macías, D., Bruno, M., Echevarría, F., Vázquez, A., García, C.M., 2008. Metereologically-induced mesoscale variability of the North-western Alboran Sea (southern Spain) and related biological patterns. Estuarine, Coastal and Shelf Science 78, 250–266.

Macías, D., Ramírez, E., García, C.M., 2010. Effect of nutrient input frequency on the structure and dynamics of the marine pelagic community. A modelling approach. Journal of Marine Research 69, 119–151.

Macías, D., Catalán, I.A., Solé, J., Morales-Nin, B., Ruiz, J., 2011. Atmospheric-induced variabiliy of hydrological and biogeochemical signatures in the NW Alboran Sea. Consequences for the spawning and nursery habitats of European anchovy. Deep-Sea Research I 58, 1175–1188.

Martin, A.P., Richards, K.J., Fasham, M.J.R., 2001. Phytoplankton production and community structure in an unstable frontal region. Journal of Marine Systems 28, 65–89.

Masó, M., Sabatés, A., Olivar, M.P., 1998. Short-term physical and biological variability in the shelf-slope region of the NW Mediterranean during the spring transition period. Continental Shelf Research 18, 661–675.

Mercado, J.M., Ramírez, T., Cortés, D., Sebastián, M., Reul, A., Bautista, B., 2006. Diurnal changes in the bio-optical properties of the phytoplankton in the Alborán Sea (Mediterranean Sea). Estuarine, Coastal and Shelf Science 69, 459–470.

Mercado, J.M., Cortés, D., García, A., Ramírez, T., 2007. Seasonal and inter-annual changes in the planktonic communities of the northwest Alboran Sea (Mediterranean Sea). Progress in Oceanography 74, 273–293.

Mercado, J.M., Cortes, D., Ramirez, T., Gomez, F., 2012. Decadal weakening of the wind-induced upwelling reduces the impact of nutrient pollution in the Bay of Malaga (western Mediterranean Sea). Hydrobiologia 680, 91–107.

Mitra, A., 2009. Are closure terms appropriate or necessary descriptors of zooplankton loss in nutrient–phytoplankton–zooplankton type models? Ecological Modelling 220, 611–620.

Morán, X.A., Estrada, M., 2001. Short-term variability of photosynthetic parameters and particulate and disolved primary production in the Alboran Sea (SW Mediterranean). Marine Ecology Progress Series 212, 53–67.

Navarro, G., Vázquez, Á., Macías, D., Bruno, M., Ruiz, J., 2011. Understanding the patterns of biological response to physical forcing in the Alborán Sea (western Mediterranean). Geophysical Research Letters 38, L23606. http://dx.doi.org/10.1029/2011GL049708.

Oguz, T., Ducklow, H.W., Malanotte-Rizzoli, P., Tugrul, S., Nezlin, N., Unluata, U., 1996. Simulation of annual plankton productivity cycle in the Black Sea by a one-dimensional physical–biological model. Journal of Geophysical Research 101, 16585–16599.

Oguz, T., Ducklow, H.W., Malanotte-Rizzoli, P., Murray, J.W., Vedernikov, V.I., Unluata, U., 1999. A physical–biochemical model of plankton productivity and nitrogen cycling in the Black Sea. Deep Sea Research I 46, 567–636.

Oguz, T., Salihoglu, B., Fach, B., 2008. A coupled plankton–anchovy population dynamics model assessing nonlinear controls of anchovy and gelatinous biomass in the Black Sea. Marine Ecology Progress Series 369, 229–256.

Prowe, A.E.F. et al., 2012. Top-down control of marine phytoplankton diversity in a global ecosystem model. Progress in Oceanography 101, 1–13.

Ramírez, T., Cortés, D., Mercado, J.M., Vargas-Yáñez, M., Sebastián, M., Liger, E., 2005. Seasonal dynamics of inorganic nutrients and phytoplankton biomass in the NW Alboran Sea. Estuarine, Coastal and Shelf Science 65, 654–670.

Raybound, V., Nival, P., Prieur, L., 2011. Short time-scale analysis of the NW Mediterranean ecosystem during summer–autumn transition: a 1D modelling approach. Journal of Marine Systems 84, 1–17.

Reul, A., Rodríguez, V., Jiménez-Gómez, F., Blanco, J.M., Bautista, B., Sarhan, T., Guerrero, F., Ruíz, J., García-Lafuente, J., 2005. Variability in the spatio-temporal distribution and size-structure of phytoplankton across an upwelling area in the NW-Alboran Sea, (W-Mediterranean). Continental Shelf Research 25, 589–608.

Rivierea, P., Pondaven, P., 2006. Phytoplanktonsize class competitions at sub-mesoscale in a frontal oceanic region. Journal of Marine Systems 60, 345–364.

Rodríguez, J., Tintoré, J., Allen, J.T., Blanco, J.M., Gomis, D., Reul, A., Ruíz, J., Rodríguez, V., Echevarría, F., Jiménez-Gómez, F., 2001. Mesoscale vertical motion and the size structure of phytoplankton in the ocean. Nature 410, 360–363.

Rubín, J.P., Cano, N., Prieto, L., García, C.M., Ruiz, J., Echevarría, F., Corzo, A., Gálvez, J.A., Lozano, F., Alonso-Santos, J.C., Escáñez, J., Juárez, A., Zabala, L., Hernández, F., García-Lafuente, J., Vargas, M., 1999. La estructura del ecosistema pelágico en relación con las condiciones oceanográficas y topográicas en el golfo de Cádiz, estrecho de Gibraltar y mar de Alborán (sector NW), en julio de 1995. Informes Técnicos del Instituto Español de Oceanografía 175, 73.

Salat, J., 1996. Review of hydrographic environmental factors that may influence anchovy habitats in Northwestern Mediterranean. Scientia Marina 60 (2), 21–32.

Siokou-Frangou, I., Christaki, U., Mazzocchi, M.G., Montresor, M., Ribera d'Alcaĺa, M., Vaque, D., Zingone, A., 2010. Plankton in the open Mediterranean Sea: a review. Biogeosciences 7, 1543–1586.

Skliris, N., Beckers, J.M., 2009. Modelling the Gibraltar Strait/Western Alboran Sea ecohydrodynamics. Ocean Dynamics 59, 489–508.

Steele, J.H., Henderson, E.W., 1992. The role of predation in plankton models. Journal of Plankton Research 14, 157–172.

Tintore, J., La Violette, P.E., Bladé, I., Cruzado, A., 1988. A study of an intense density front in the eastern Alborán Sea: the Almerian–Oran front. Journal of Physical Oceanography 18, 1384–1397.

Tintore, J., Gomis, D., Alonso, S., Parrilla, G., 1991. Mesoscale dynamics and vertical motion in the Alborán Sea. Journal of Physical Oceanography 21, 811–823.
Travers, M., Shin, Y.-J., 2010. Spatio-temporal variability in fish-induced predation mortality on plankton: a simulation approach using a coupled trophic model of the Benguela ecosystem. Progress in Oceanography 84, 118–120.
Vanderploeg, H.A., Scavia, D., 1979. Calculation and use of selectivity coefficients of feeding: zooplankton grazing. Ecological Modelling 7, 135–149.
Viudez, A., Pinot, J.M., Haney, R.L., 1998. On the upper layer circulation in the Alborán Sea. Journal of Geophysical Research 103, 21653–21666.